



HAL
open science

Reliability of B-mode ultrasound and shear wave elastography in evaluating sacral bone and soft tissue characteristics in young adults with clinical feasibility in elderly

Maher Abou Karam, Ekaterina Mukhina, Nils Daras, Isabelle Rivals, H el ene Pillet, Wafa Skalli, Nathana el Connesson, Yohan Payan, Pierre-Yves Rohan

► To cite this version:

Maher Abou Karam, Ekaterina Mukhina, Nils Daras, Isabelle Rivals, H el ene Pillet, et al.. Reliability of B-mode ultrasound and shear wave elastography in evaluating sacral bone and soft tissue characteristics in young adults with clinical feasibility in elderly. *Journal of Tissue Viability*, 2023, 31 (2), pp.245-254. 10.1016/j.jtv.2022.02.003 . hal-04018121

HAL Id: hal-04018121

<https://hal.science/hal-04018121>

Submitted on 9 Mar 2023

HAL is a multi-disciplinary open access archive for the deposit and dissemination of scientific research documents, whether they are published or not. The documents may come from teaching and research institutions in France or abroad, or from public or private research centers.

L'archive ouverte pluridisciplinaire **HAL**, est destin ee au d ep ot et  a la diffusion de documents scientifiques de niveau recherche, publi es ou non,  emanant des  tablissements d'enseignement et de recherche fran ais ou  trangers, des laboratoires publics ou priv es.



Distributed under a Creative Commons Attribution 4.0 International License

Reliability of B-mode Ultrasound and shear wave elastography in evaluating sacral bone and soft tissue characteristics in young adults with clinical feasibility in elderly

**Maher Abou Karam ^{a *}, Ekaterina Mukhina ^b, Nils Daras ^a, Isabelle Rivals ^{c d},
Helene Pillet ^a, Wafa Skalli ^a, Nathanaël Connesson ^b, Yohan Payan ^b, Pierre-Yves
Rohan ^a**

^a Institut de Biomécanique Humaine Georges Charpak, Arts et Métiers Institute of technology, 151 bd de l'Hôpital, 75013 Paris, France

^b Univ. Grenoble Alpes, CNRS, Grenoble INP, TIMC-IMAG, Grenoble, France

^c Sorbonne Université, INSERM, UMRS1158 Neurophysiologie Respiratoire Expérimentale et Clinique, Paris, France

^d Equipe de Statistique Appliquée, ESPCI Paris, PSL Research University, Paris, France

1 Keywords: pressure ulcer, sacrum, medial sacral crest, elderly, ultrasound, shear wave elastography, elasticity,
2 reliability

3 *List of abbreviations:*

4 B-mode, Brightness mode; CI, confidence interval; CT, Computed tomography; FE, Finite element; HT, Hypodermis
5 thickness; hSWE, hypodermis shear wave elastography; HE, Medial sacral crest height; ICC, intraclass correlation
6 coefficient; IT, ischial tuberosity; MRI, Magnetic resonance imaging; MSC, Medial sacral crest; mSWE, muscle shear
7 wave elastography; OA, Medial sacral crest opening angle; PSIS, Posterior superior iliac spine; PU, Pressure ulcer;
8 ROC, Medial sacral crest radius of curvature; ST, Skin thickness; SWE, Shear wave elastography; sSWE, Skin shear
9 wave elastography; US, ultrasound.

10

11 **Abstract**

12 *Background:* Physiologic aging is associated with loss of mobility, sarcopenia, skin atrophy and loss of elasticity.
13 These factors contribute, in the elderly, to the occurrence of a pressure ulcer (PU). Brightness mode ultrasound (US)
14 and shear wave elastography (SWE) have been proposed as a patient-specific, bedside, and predictive tool for PU.
15 However, reliability and clinical feasibility in application to the sacral region have not been clearly established.

16 *Method:* The current study aimed to propose a simple bedside protocol combining US and SWE. The protocol was
17 first tested on a group of 19 healthy young subjects by two operators. The measurements were repeated three times.
18 Eight parameters were evaluated at the medial sacral crest. Intraclass Correlation Coefficient (ICC) was used for
19 reliability assessment and the modified Bland Altman plot analysis for agreement assessment. The protocol was then
20 evaluated for clinical feasibility on a healthy older group of 11 subjects with a mean age of 65 ± 2.4 yrs.

21 *Findings:* ICC showed poor to good reliability except for skin SWE and hypodermis thickness with an ICC (reported
22 as: mean(95%CI)) of 0.78(0.50-0.91) and 0.98(0.95-0.99) respectively. No significant differences were observed
23 between the young and older group except for the muscle Shear Wave Speed (SWS) (respectively 2.11 ± 0.27 m/s vs
24 1.70 ± 0.17 m/s).

25 *Interpretation:* This is the first protocol combining US and SWE that can be proposed on a large scale in nursing
26 homes. Reliability, however, was unsatisfactory for most parameters despite efforts to standardize the protocol and
27 measurement definitions. Further studies are needed to improve reliability.

28

29 **Introduction**

30 Tissue morphology, mechanical properties, physiology, and repair properties can all change over time as a result of
31 aging, lifestyle, chronic injury, or disease. Over a bony prominence, these changes - associated with a mechanical load
32 - can lead to a localized injury known as a “pressure ulcer” [1].

33 The prevalence of this lesion ranges between 9% [2] and 15% [3] in long term care or hospitalized patients , and is
34 most frequently observed over the sacrum or the heel. Two thirds of PU are observed in patients above 70 years of age
35 [4]. The occurrence of PU is associated with significant increase in hospital costs, length of stay and, most importantly,
36 an increased risk of death. [5]–[7].

37 While numerous and efficient therapies have been developed, prevention remains the center of interest of all healthcare
38 professionals and thus of researchers [4]. However, current practices in PU prevention are far from satisfactory with
39 more than 85% lack in documented repositioning care plan. This is majorly due to the lack of staff and time [2]. PU
40 prevention protocols are based on risk assessment tools or scales (Norton scale, Braden scale...) [8]. The impact of
41 these tools on the incidence of PU remains uncertain and fail to meet the needs of all patients in different clinical
42 settings [7].

43
44 The process of aging is associated with physiological changes including sarcopenia, osteoporosis, progressive increase
45 in blood glucose and skin atrophy [9]. The decrease in muscular power has a high impact on the performance of daily
46 activities even in healthy older persons leading to increased immobility [10]. In consequence, the elderly are
47 considered at risk of developing PU and therefore, a target group for preventive screening protocols. Several bedside
48 technologies combined with assessment tools were investigated for early detection of PU, especially in long term care
49 facilities. High frequency ultrasound (HFUS) was particularly studied, given its accessibility and capacity to detect
50 preclinical superficial skin changes, mainly the presence of fluid/oedema at different levels of the skin [11]. However,
51 a randomized controlled trial [12] failed to demonstrate that HFUS was an effective strategy for predicting the
52 development of Category/Stage I PU s of the heel or sacrum compared with a focused physical assessment. Also, a
53 systematic review [13] evaluated HFUS among other technologies. Despite giving meaningful and consistent results,
54 it could not be recommended due to lack of reliability of protocols, being limited to detecting macroscopic level tissue
55 damage, and its training requirements for image interpretation.

56 In terms of etiology/pathophysiology, studies based on both *in vitro* (cell models) and *in vivo* (animal models)
57 approaches have demonstrated that at least two damage mechanisms, are involved in the development of PU: first,
58 compression damage due to tissue ischemia/reperfusion initiated by local, moderate and persistent mechanical loads;
59 secondly, direct deformation damage above a threshold level related to shear strain; even for a short period of time
60 (during transfer from bed to a wheelchair for example) [14]. These results suggest the presence of a direct link between
61 mechanical determinants and biological processes leading to tissue damaging and, in fine, necrosis.

62 Based on the rationale that elucidating the relationship between external loads and internal local stresses and strains
63 within loaded soft tissues has the potential of improving the management and prevention of PUs, several Finite
64 Element (FE) models of the buttocks have been proposed in the literature. Models are mostly based on the
65 segmentation of MRI or CT scan sequences [15]–[18]. However, the use of MRI and CT scans is limited due to cost,
66 accessibility, and time [19]. In this perspective, brightness mode (B-mode) ultrasound (US) imaging was proposed as
67 an alternative to MRI or CT-scan. Feasibility, reproducibility, and its use for personalized FE models were investigated
68 mainly over the ischial tuberosity [19]–[23].

69 Recent studies [19], [24], [25] proposed B-mode US for the evaluation of biomechanical risk of PU in a seated position
70 by assessing, among other parameters, tissue thickness changes in different positions. On the other hand, ultrasound
71 elastography, a relatively new method that shows structural changes in tissues following application of physical stress
72 can be used in the examinations of musculoskeletal system [26]. Shear wave elastography (SWE) uses focused
73 ultrasonic beams, to remotely generate mechanical vibration sources radiating low-frequency, shear waves inside
74 tissues [27]. It allows a bedside evaluation of the local mechanical properties of soft biological tissues by assessing
75 shear modulus [28]–[30]. Experiments demonstrated that ultrasound elastography is a promising technique for PU
76 detection, especially at an early stage of the pathology, when the disease is still visually undetectable [28].

77 Previous studies investigating the combination of B-mode US and SWE elastography in the context of PU prevention
78 focused on potential changes of tissue stiffness during prolonged loading [31] or tissue characteristics in different body
79 postures [32].

80

81 The current study aimed to propose and test a bedside B-mode US and SWE protocol that can be used as a risk
82 assessment tool for sacral PU in elderly. The protocol was designed for the evaluation of bone geometry, tissue
83 morphology and mechanical characteristics over the sacrum. Reliability and reproducibility of our protocol were tested

84 on a healthy young adults group. The protocol was then applied on a group of healthy older people to assess for clinical
85 feasibility.

86

87 **Materials and methods**

88 **1. Data Collection**

89 The current study was approved by the ethics committee (Comité de protection des Personnes CPP NX06036) and
90 each subject gave an informed consent. For the reproducibility analysis 19 young healthy subjects participated to the
91 experiment, 8 women and 11 men (Age: 25.7 ± 3.8 yrs, Weight: 75.2 ± 16.4 kg, BMI: 24.5 ± 4.9 kg/m²). For the
92 elderly group 11 healthy subjects, 7 women and 4 men were recruited (Age: 65 ± 2.4 yrs, Weight: 72.5 ± 18.6 kg,
93 BMI: 25.34 ± 5 kg/m²). Exclusion criteria included: the presence of chronic or acute low back pain, history of lower
94 spine surgery or sacral PU, and the presence of PU skin signs at the moment of the acquisition.

95

96 *Ultrasound acquisition protocol*

97 B-mode US images and shear wave elastography (SWE) videos were obtained using a commercial device
98 (SupersonicMach30, SuperSonic Imagine, France). Two probes were used, the curvilinear (SuperCurved C6-1X) with
99 low frequency (1 to 6 MHz allowing increased depth visualization) and large field of view, and the linear (SuperLinear
100 L10-2) probe with a higher frequency (2 to 10 MHz allowing superficial layers visualization). The general mode and
101 penetration optimization were chosen for all acquisitions.

102 A standardized - tissue and musculoskeletal US/SWE over the sacral region - protocol was developed and was first
103 pilot tested on a sample of three healthy young volunteers, consequently, adjustments were made. The definitive
104 protocol is described thoroughly in Appendix 1.

105 Acquisitions were taken in the lying prone position. After anatomic palpation of the two posterior superior iliac spines
106 (PSIS), the curvilinear probe was first used in B-mode to recognize the anatomic region of interest: the MSC. An
107 image was captured to assess bone anatomy and the skin was marked with a tape. Switching to the linear probe, the
108 second image captured the skin and hypodermis at the level of the MSC. The third part, also using the linear probe at
109 the marked skin level, was a series of three videos (of 10 seconds each) in SWE mode with a region of interest (ROI)
110 including both skin and hypodermis. For the fourth and last part, three SWE videos of the gluteus maximus muscle

111 were taken lateral to the sacro-coccygeal region at the lower part of the sacrum. The images/videos using the linear
 112 probe were taken with minimal applied pressure, using a thick gel layer and making sure it was visible on the US
 113 image. A summary of the acquisition protocol and images are shown in figure 1.

114

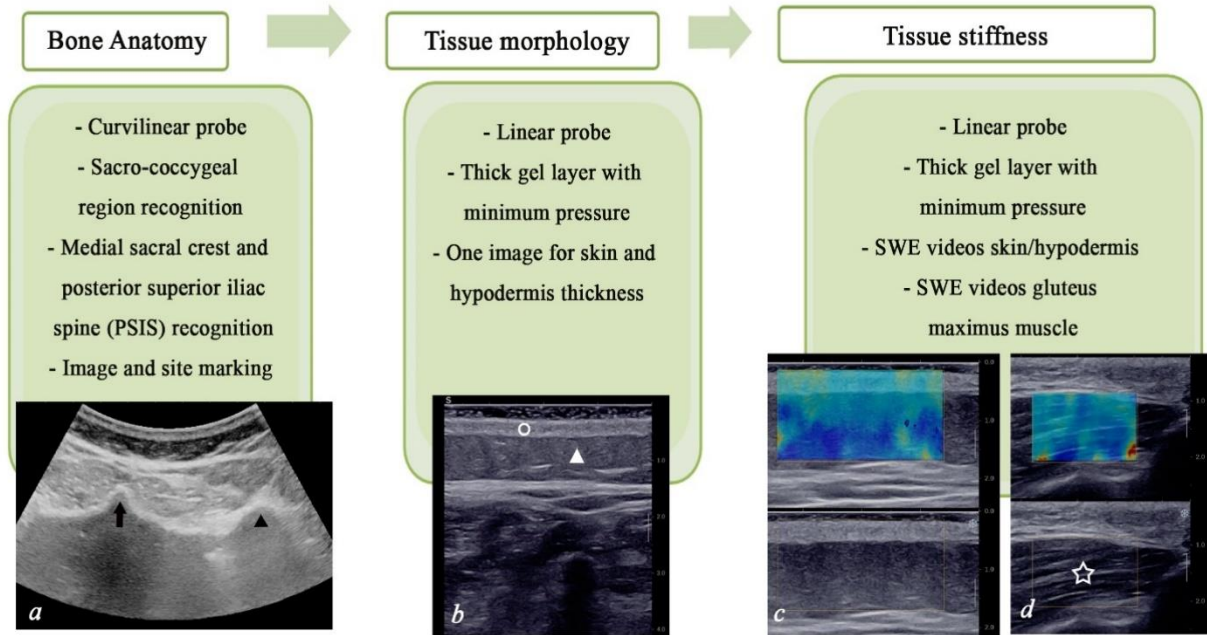
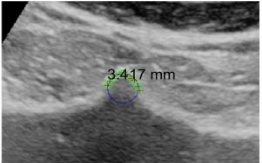
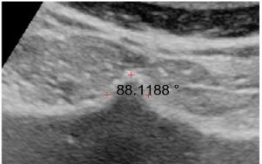
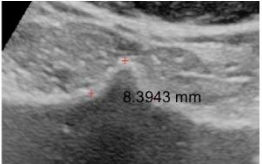
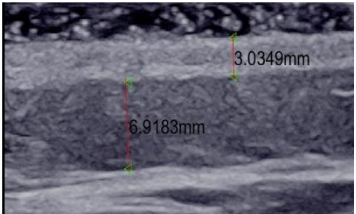
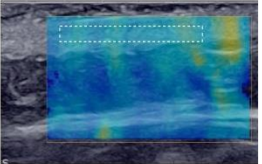
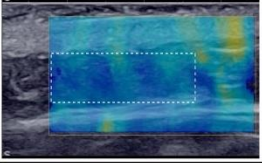
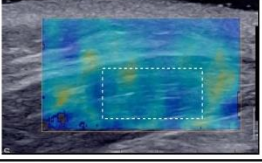


Fig. 1. US acquisition protocol of the sacral region in the transverse view. In B-mode: the medial sacral crest (arrow) at the level of the PSIS (black triangle) (a), skin (circle) and adipose tissue (white triangle) over MSC (b); in SWE mode: the skin and adipose tissue (c), gluteus maximus muscle (star) (d).

115 *Parameter estimation*

116 To reduce acquisition time, processing and measurements for images/videos were done separately using a custom
 117 software written in Matlab (R2019a) (MathWorks, Inc, Natick MA). In total 8 parameters were measured using the
 118 images/videos captured during each acquisition. First, the bone anatomy image (fig.1a) was used to measure the MSC
 119 radius of curvature (ROC), opening angle (OA), and height (HE). Then, the second image (fig.1b) was used to measure
 120 the skin thickness (ST) and the hypodermis thickness (HT). For the SWE videos of the third (fig.1c) and fourth (fig.1d)
 121 part of the acquisition, images were extracted and processed using a separate written code [33]. The average value of
 122 the images of each video was calculated and then, the average of the three videos determined the shear wave velocity
 123 of one acquisition for: the skin (sSWE), the hypodermis (hSWE), and gluteus maximus muscle (mSWE). Details about
 124 the definitions and recommendations for these measurements are reported in table 1.

Table 1. Description of parameter measurement post acquisition using a customized MATLAB algorithm

| | Parameter name | Description | Post-processing |
|---|---------------------------|---|---|
| <i>Bone anatomy (curvilinear probe - B-mode)</i> | Radius of curvature (ROC) | 10 points distributed equally on both sides of the tip of MSC ; the circle plotted was viewed to ensure it captures the shape of the tip (19) |  |
| | Opening angle (OA) | 3 points: one on the middle of the MSC tip and two bilateral points |  |
| | Height (HE) | 3 points: the geometry of the MSC could be compared to a triangle, the tip is the highest point of the triangle and two points for the base of the MSC; the distance from the upper point to the base is the HE |  |
| <i>Tissue morphology (linear probe - B-mode)</i> | Skin thickness (ST) | 2 points: the upper limit marked by the most superficial, homogenous, and continuous line of the epidermis; lower border marked by the transition between dermis and hypochoic adipose tissue |  |
| | Hypodermis thickness (HT) | 2 points: thickest hypochoic region under the skin; hyperechoic muscle fascia marks the lower border | |
| <i>Tissue stiffness (linear probe - SWE mode)</i> | SWE hypodermis (hSWE) | Region of interest (ROI): largest, most homogenous SWE signal |  |
| | SWE skin (sSWE) | |  |
| | SWE gluteus muscle (mSWE) | |  |

126 **2. Method Evaluation**

127 *Sample size and Reliability assessment*

128 All the data were analyzed with the IBM SPSS for Windows (Version 27.0. Armonk, NY: IBM Corp).

129 The reliability study was conducted on the young, healthy group by two operators: a physician and an engineer. Both
130 operators received extensive training consisting of two phases: first, measurements were repeated until reaching
131 adequate reproducibility compared with an expert sonographer then, deviations were assessed, and possible problems
132 were determined and corrected.

133 The operators were asked to repeat the protocol three times on each subject, i.e., captured three images for each of the
134 bone geometry parameters and tissue morphology, and nine SWE videos for each tissue stiffness parameter.

135 The reliability of our protocol was assessed by calculating the intra class correlation coefficient (ICC) for within-
136 operator and between-operator for the young subjects group [34]. The minimum sample size required for this test-
137 retest reliability study was estimated based on the recommendations made in Bujang et al [35]. With three observations
138 per subject, a minimum sample size of 15 is required to detect an ICC value of 0.5 with power of 90% when taking a
139 type I error risk of 5% (table 1a of [35]).

140 Given that ultrasound acquisition is highly operator dependent, and that the processing/measurement of a given
141 image/video (i.e. definitions of parameters) might also differ from one operator to another, we decided to quantify the
142 variability first at processing level, and then at both processing and acquisition level. First, the two operators processed
143 and measured one acquisition conducted by the physician on all subjects. Each operator repeated measurement of the
144 same image/video three times, allowing an intra-image analysis [36]. For this analysis, the ICC model 3 (2-way mixed)
145 was chosen for within-operator reliability, and ICC model 2 (2-way random) for between-operator reliability with
146 absolute agreement type and single measure [37]. For between operator reliability, values of one of the three
147 measurement, chosen randomly for each operator, was used. Then, each operator processed and measured their own
148 acquisitions allowing an inter-image analysis [36]. The same model and type for within-operator ICC (2-way mixed
149 and absolute agreement) were used with single measure, and for between-operator reliability also the ICC model 2
150 was used but with consistency agreement type and single measure since different images are compared. Also, for
151 between operator reliability, values of one of the three measurements, chosen randomly for each operator, was used.
152 This procedure was conducted for each parameter and the ICC with 95% confidence interval was reported. Values
153 less than 0.5, between 0.5 and 0.75, between 0.75 and 0.9, and greater than 0.90 indicated poor, moderate, good, and

154 excellent reliability, respectively [37].

155 *Agreement assessment*

156 The modified Bland Altman plot analysis for continuous measures [38] was used as a measure of the level of agreement
157 within and between operators for both the intra-image and inter-image analysis. In the absence of a gold standard, the
158 value of each measurement was compared to the average of all measurements for one subject (bias line equal to zero).
159 The difference between each observer and the overall mean for a subject is estimated. The 95% level of agreement
160 with the mean is estimated as $\pm 2 \times$ Standard deviation (SD), where SD represents the square root of the variance of
161 the differences.

162 *Healthy young adults vs healthy elderly*

163 The same protocol was conducted once (one acquisition and measured once) on the older group by one operator: the
164 physician. For the young adults group data, the measurements of one of the three acquisitions collected by the
165 physician were chosen randomly. Normality was checked with the Shapiro–Wilk test and the equality of variance was
166 assessed with the Levene's test. If both normal distribution and equality of variance of the different groups could be
167 assumed, data were reported per parameter and per group as mean ± 1 SD and groups (young versus old) were
168 compared using the student t-test. In case the normality or equality of variance assumption was violated, groups were
169 compared with the Wilcoxon test. For all the tests, the significance level was set at 0.05 *a priori*.

170 **Results**

171 *Reliability assessment*

172 Within operator and between operator ICC with the 95% confidence interval, for both the intra and inter-image analysis
173 for all parameters, are reported in table 2. First in the intra-image analysis, all ICC confidence interval values showed
174 good to excellent reliability for within operator, except for the ROC, and the OA of the MSC for the physician with
175 moderate to excellent reliability. For between operator ICC the following parameters: HE, hypodermis thickness, SWE
176 skin, SWE hypodermis, SWE muscle, showed good to excellent reliability. The ICC for the OA and the skin thickness
177 showed moderate to excellent reliability. For the inter-image analysis, within operator ICC showed excellent reliability
178 for the hypodermis thickness parameter for both operators. The physician (operator 1) showed good to excellent

179 reliability for the ROC and HE. For the SWE skin parameter he showed moderate to excellent reliability; for the
 180 opening angle parameter moderate to good reliability; for the remaining parameters poor to good reliability. The
 181 engineer (operator 2) showed moderate to excellent reliability for the ROC, SWE skin, SWE hypodermis, and SWE
 182 muscle parameters. For the opening angle parameter, the engineer showed moderate to good reliability; for the HE,
 183 skin thickness poor to good reliability. The between operator ICC also showed excellent reliability for the hypodermis
 184 thickness. The ICC for SWE skin parameter showed moderate to excellent reliability. The ICC of the remaining
 185 parameters showed poor to good reliability.

186
 187 *Table 2. Reliability assessment results with Intraclass correlation coefficient ICC for both intra-image and inter-image analysis*
 188 *for both operators: 1 the physician and 2 the engineer.*
 189

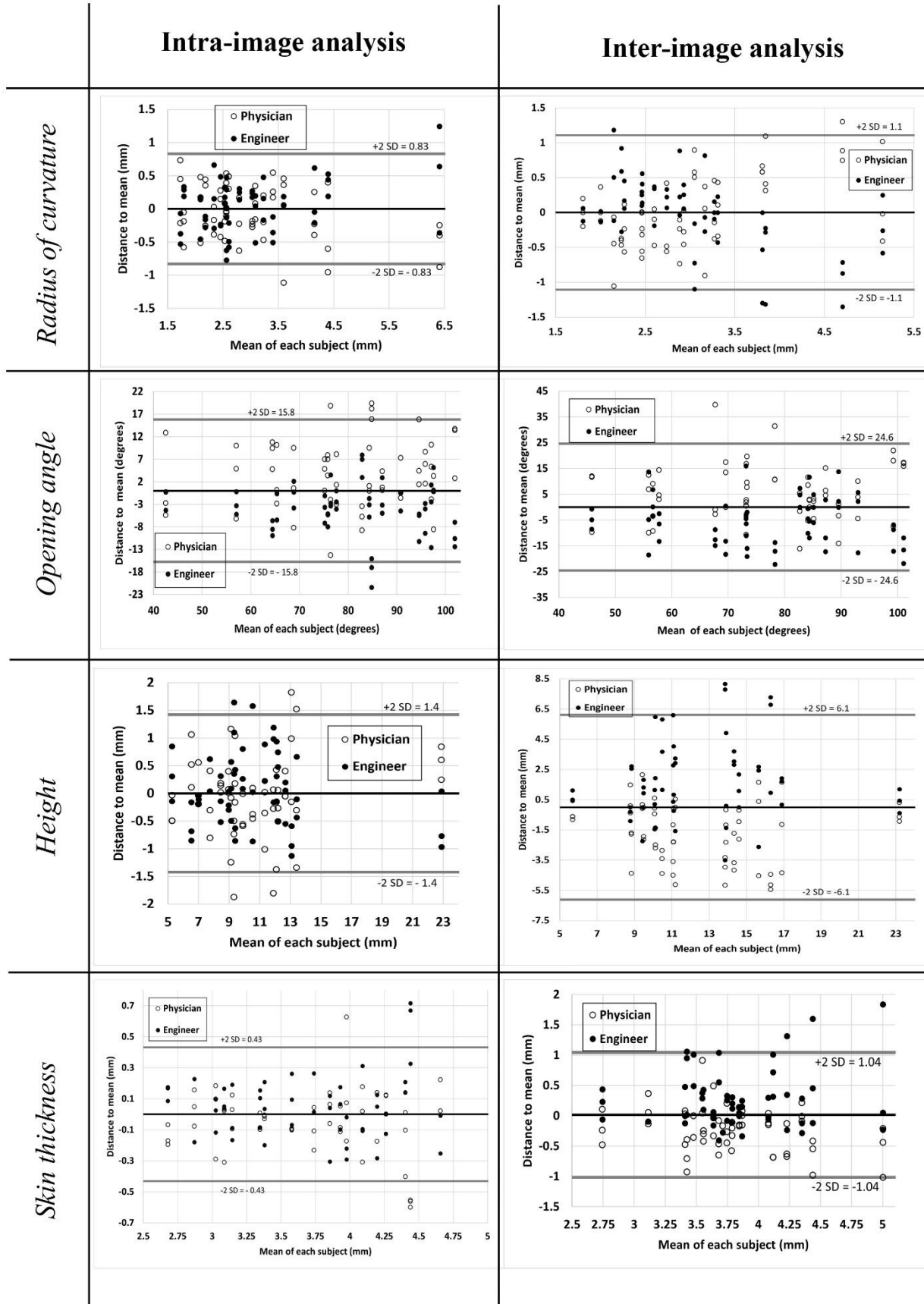
| Parameter | Operator | Intra-image analysis | | Inter-image analysis | |
|----------------------|----------|---------------------------------|----------------------------------|---------------------------------|----------------------------------|
| | | Within operator ICC (95% CI) | Between operator ICC (95% CI) | Within operator ICC (95% CI) | Between operator ICC (95% CI) |
| Radius of curvature | 1 | 0.86(0.68-0.94) | 0.84(0.64-0.94) | 0.90(0.79-0.96) | 0.69(0.34-0.87) |
| | 2 | 0.93(0.84-0.97) | | 0.76(0.53-0.90) | |
| Opening angle | 1 | 0.86(0.66-0.94) | 0.81(0.57-0.92) | 0.74(0.53-0.89) | 0.58(0.17-0.82) |
| | 2 | 0.96(0.91-0.98) | | 0.73(0.50-0.88) | |
| Height | 1 | 0.97(0.93-0.99) | 0.97(0.92-0.99) | 0.89(0.78-0.96) | 0.74(0.43-0.89) |
| | 2 | 0.98(0.95-0.99) | | 0.69(0.45-0.87) | |
| Skin thickness | 1 | 0.94(0.87-0.97) | 0.88(0.73-0.95) | 0.71(0.49-0.87) | 0.53(0.09-0.80) |
| | 2 | 0.95(0.88-0.98) | | 0.59(0.32-0.80) | |
| Hypodermis thickness | 1 | 0.99(0.99-1.00) | 0.99(0.99-1.00) | 0.98(0.96-0.99) | 0.98(0.95-0.99) |
| | 2 | 0.99(0.99-1.00) | | 0.99(0.98-1.00) | |
| SWE skin | 1 | 0.99(0.99-1.00) | 0.99(0.99-1.00) | 0.83(0.67-0.93) | 0.78(0.50-0.91) |
| | 2 | 0.99(0.99-1.00) | | 0.85(0.72-0.94) | |
| SWE hypodermis | 1 | 0.99(0.98-1.00) | 0.98(0.94-0.99) | 0.70(0.46-0.86) | 0.65(0.27-0.85) |
| | 2 | 0.98(0.97-0.99) | | 0.80(0.63-0.91) | |
| SWE muscle | 1 | 0.96(0.88-0.99) | 0.93(0.79-0.98) | 0.71(0.41-0.90) | 0.41(-0.22-0.80) |
| | 2 | 0.98(0.96-1.00) | | 0.84(0.63-0.95) | |

190

191

192 *Agreement assessment*

193 The modified Bland Altman agreement plots for both the intra and inter image analysis are reported in figure 2. The
194 95% limits of agreement with the mean varied from the intra to the inter-image analysis as follows: for the ROC from
195 ± 0.83 mm to ± 1.1 mm; for the opening angle from ± 15.8 degrees to ± 24.8 degrees; for the HE from ± 1.4 mm to ± 6.1
196 mm; for the skin thickness from ± 0.43 mm to ± 1.04 mm; for the hypodermis thickness from 0.57 mm to 1.4 mm; for
197 the SWE skin from ± 0.03 m/s to ± 0.33 m/s; for the SWE hypodermis from ± 0.06 m/s to ± 0.29 m/s; and for the SWE
198 muscle from ± 0.08 m/s to ± 0.25 m/s.



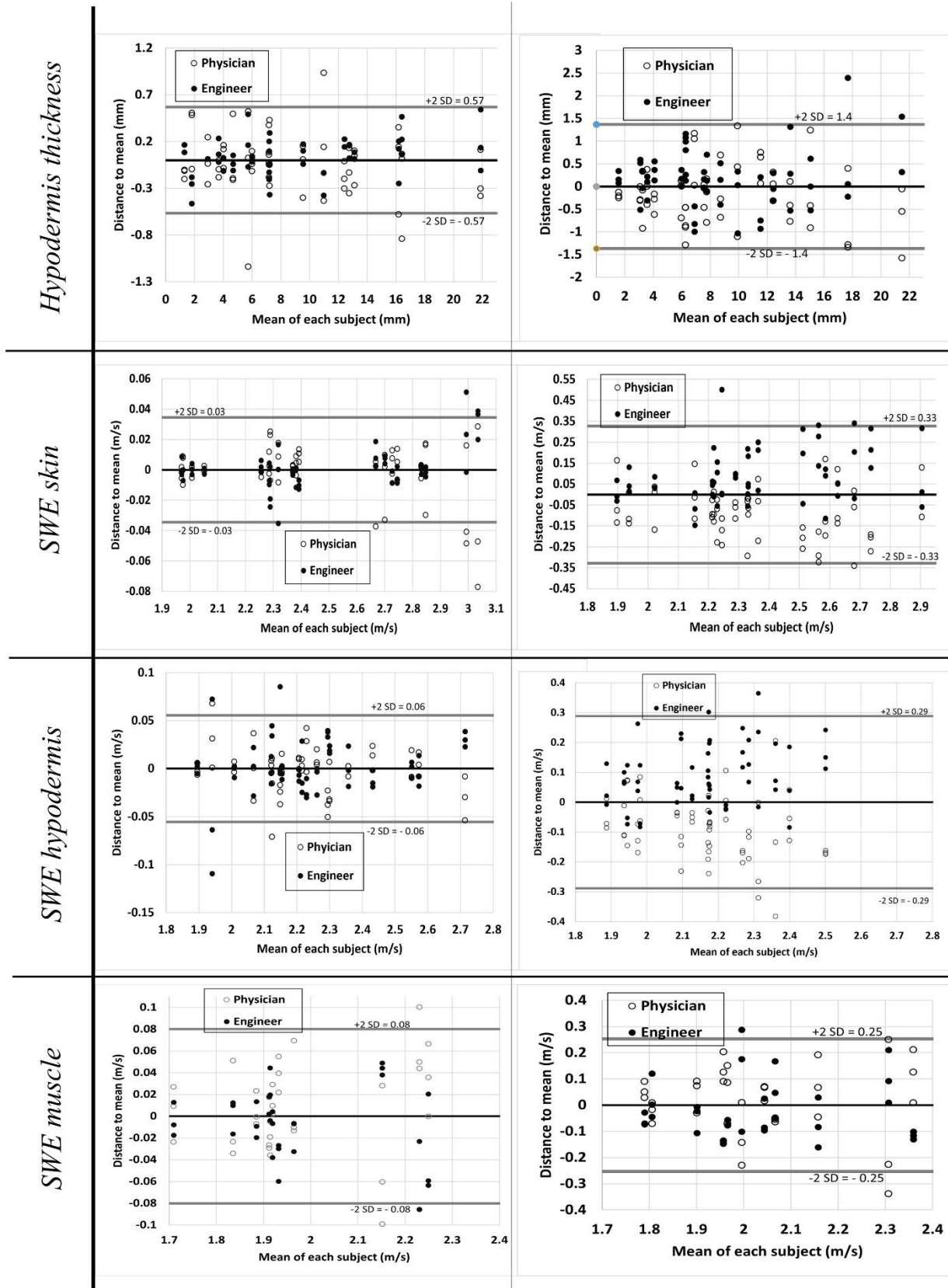


Fig. 2. Agreement plots with the mean of measurements for the intra-image and inter-image analyses for the 8 parameters

201 *Healthy Young adults VS healthy elderly*

202 The results of means, normality tests and Student’s t-test test are reported in table 3. There was insufficient evidence
 203 to claim that the distributions were not normal or that the variances were not equal. Based on the results of the student
 204 t-test, we concluded that there is a statistically significant difference only for the mSWE (2.11 ± 0.27 m/s for the young
 205 adults group vs 1.70 ± 0.17 m/s for the elderly, p-value = 0.001). Because of the relatively small sample size, the
 206 sample means for each parameter were also compared using the Wilcoxon signed rank test. The conclusions were the
 207 same i.e., there is a statistically significant difference only for the mSWE.

208 Images reported in figure 2 show observations for the older group subjects that diverged from the group. The upper
 209 and lower limits for skin and hypodermis SWE were found in a 62-year-old male subject with a BMI of 39.1 kg/m^2
 210 (fig.2a) and a 67-year-old male with a BMI of 27.4 kg/m^2 (fig.2b), respectively. A 62-year-old female elderly with a
 211 BMI of 22.3 kg/m^2 (fig.2c) showed a heterogeneous distribution of hypodermis thickness over the MSC.

212

213 *Table 3. Mean of each parameter for the young adults group and healthy elderly, normality using Shapiro-wilk*
 214 *test and comparison using Student’s t-test.*

| Parameter | | Young adults | | Healthy elderly | | Student’s t-test p-value |
|--------------------|------------|-------------------|---------------------------|-------------------|---------------------------|--------------------------|
| | | Mean \pm SD | Shapiro Wilk test p-value | Mean \pm SD | Shapiro Wilk test p-value | |
| Bone anatomy (MSC) | OA (°) | 80.32 ± 21.06 | 0.628 | 79.54 ± 19.19 | 0.509 | 0.920 |
| | HE (mm) | 10.39 ± 4.45 | 0.119 | 8.20 ± 2.94 | 0.293 | 0.159 |
| | ROC (mm) | 2.90 ± 1.21 | 0.191 | 2.19 ± 0.17 | 0.550 | 0.088 |
| Tissue morphology | ST (mm) | 3.61 ± 0.55 | 0.982 | 3.30 ± 0.53 | 0.215 | 0.147 |
| | HT (mm) | 8.67 ± 5.21 | 0.380 | 6.08 ± 3.56 | 0.457 | 0.156 |
| Tissue stiffness | sSWE (m/s) | 2.27 ± 0.28 | 0.087 | 2.22 ± 0.55 | 0.295 | 0.800 |
| | hSWE (m/s) | 2.06 ± 0.16 | 0.497 | 1.98 ± 0.33 | 0.437 | 0.465 |
| | mSWE (m/s) | 2.11 ± 0.27 | 0.128 | 1.70 ± 0.17 | 0.758 | 0.001 |

215

216

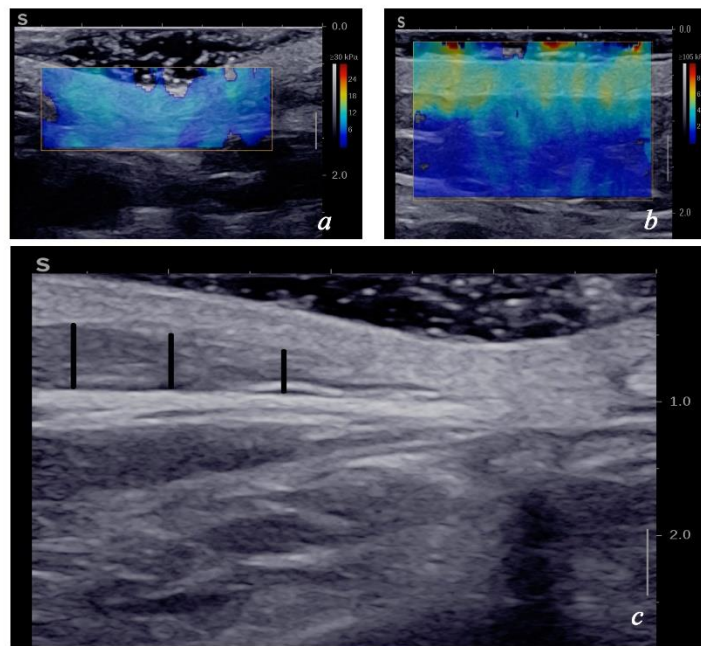


Fig. 3. Observations in the elderly group: lowest and highest skin/hypodermis SWE signal (a,b respectively), hypodermis heterogeneous thickness distribution over the MSC (black vertical lines) (c)

217 Discussion

218 This study aimed to evaluate the use of B-mode US and SWE in the assessment of bone geometry, tissue morphology
219 and tissue stiffness in the context of sacral PU prevention in elderly. A protocol was developed to evaluate the region
220 over the MSC. It was tested for reliability on a group of 19 healthy young subjects by two operators: a physician and
221 an engineer. Afterwards, the protocol was tested on a group of 11 healthy older people by the physician only. The
222 parameters evaluated by our protocol were: the radius of curvature (ROC), opening angle (OA), and height (HE) of
223 the MSC for the bone geometry; the skin thickness (ST), and hypodermis thickness (HT) for the tissue morphology;
224 skin shear wave velocity (sSWE), hypodermis shear wave velocity (hSWE), and muscle shear wave velocity (mSWE)
225 for tissue stiffness.

226

227

228

229 1. Reliability study

230 The intra-image analysis was first conducted to assess the operators understanding and reliability of measuring each
231 parameter. Within-operator ICC was good to excellent for all parameters for the engineer. For the physician, most
232 parameters showed good to excellent reliability except for the ROC (CI 0.68-0.94) and OA (CI 0.66-0.94), showing
233 moderate to excellent reliability. This might be due to an unclear definition of these two parameters. While the ROC
234 is measured by placing points on the tip of MSC, the position of the start and ending points are not always clear.
235 Between operator ICC, for the intra-image analysis, showed good to excellent reliability for all parameters except
236 ROC, OA, ST with moderate to excellent reliability. These results also highlight the difficulty in choosing the points
237 for the ROC and OA. For the ST parameter, although the skin is a continuous layer over the hypodermis, both stratum
238 corneum : the most superficial layer of the epidermis, and the reticular layer: the lower part of the dermis, are wavy
239 layers and thus might affect ST measurement depending on the part of the image chosen to assess ST [39]. The inter-
240 image analysis aimed to test whether operators are capable of successfully repeating an acquisition three times and
241 reproducing the acquisition protocol. Because acquisitions measured were not the same, ICC results were expected to
242 have lower values. The discussion will involve only the parameters that showed good to excellent reliability on the
243 intra-image analysis. First the HE parameter, within operator reliability was good to excellent for the physician but
244 low to good for the engineer. A possible explanation might be that the acquisitions were not taken at the same level
245 over the MSC. Another explanation is the fact that, in terms of anatomy, the sacrum is the most variable portion of the
246 spine. In fact, the MSC is formed by the fusion of the spinous processes of the first three to four sacral vertebrae, and
247 therefore bone morphology might differ from a level to another [40]. In this perspective, an emphasis should be on
248 taking the acquisition at the level of the two PSIS, since it is a fixed, palpable and US visible anatomic landmark (using
249 the curvilinear probe). Also, the only study, that the authors found in the literature, that included US and SWE tissue
250 evaluation of the sacral region reported neither the protocol of measurement nor the US anatomic landmark used
251 during acquisition [31]. The authors think that this biased the results since the anatomy of the sacrum is complex and
252 irregular [40], [41].

253 For the shear wave velocity: within operator and between operator ICCs showed moderate to excellent reliability for
254 the skin; low to good reliability for hypodermis and muscle for both within and between operator ICCs. Possible
255 reasons include signal instability and inhomogeneity associated with tissue depth and operator's experience. Another
256 reason might be tissue anisotropy, therefore tissue SWE signal depends on the orientation of the probe relative to the

257 layer tested. Also, this affects much more muscular fibres since they're organised with a geometric alignment
258 compared with the less structured adipose tissue or skin [42]. This explains the larger gap observed in the CI of between
259 operator ICC for the mSWE (table 2).

260 The agreement plots were drawn to assess clinical significance of difference between measurements even when a
261 parameter showed good reliability [38]. In the absence of a gold standard imaging tool in our study the level of
262 agreement necessary for confident usage remains uncertain. However, we hypothesized that the clinical difference
263 between different groups is significantly higher than the uncertainty of the measurements. For the bone geometry
264 parameters, previous studies focused on ischium morphology and its impact on internal soft tissue strain thus on the
265 occurrence of PU using mainly FE models [23], [43]. Our aim was to combine the three bone parameters : ROC, OA,
266 and HE to differentiate a sharp tip from a flat tip [44]. For our knowledge, no research was conducted on the impact
267 of the shape of the MSC on surrounding tissue deformation. In fact, reliability of bone morphology assessment using
268 ultrasound is controversial: Akins et al [19] found good between operator reliability for ischial tuberosity (IT) radius
269 of curvature but they only reported the average ICC = 0.712 , while Swaine et al [20] found poor reliability for
270 estimating inferior curvature of the IT in both its short and long axis. The methodology for our protocol combining an
271 intra-image and-inter image analysis seemed promising but, with lack of reliability in the results and no clinical
272 baseline for the MSC morphology, no interpretation could be given to the agreement plots reported in figure 2 for
273 these parameters.

274 For tissue morphology parameters, skin thickness showed low reliability and a 95% CI of agreement with the mean of
275 ± 1.04 mm for the inter-image analysis. With a maximum skin thickness reported in the literature of 4mm [39] this
276 parameter needs further investigation before clinical use. A possible solution might be to tell operators to measure the
277 ST directly over the MSC. In this perspective and since the linear probe is limited in depth and field of view, the first
278 acquisition using the curvilinear probe is crucial for identifying and marking the level of the MSC, but also its exact
279 position over the spine midline. In fact, previous studies investigating the inter-operator reliability of tissue thickness
280 measurement over IT showed : excellent reliability for total thickness with an average ICC=0.948, also without
281 reporting the confidence interval [19] ; moderate to excellent reliability (0.60-0.95) for skin and fat thickness [20]. To
282 our knowledge, no study investigated the reliability of measuring tissue thickness using US over the sacrum. On the
283 other hand, hypodermis thickness parameter showed excellent reliability and a 95% CI of agreement with the mean of
284 ± 1.4 mm for the inter-image analysis. Since hypodermis thickness is variable, and mainly related to body mass index

285 [45] with a value exceeding sometimes 50 mm over lumbar spine [46], the clinical significance of this agreement
286 seems plausible. However, the interpretation depends on another factor: the homogeneity of the distribution of the
287 hypodermis over the sacrum. This is going to be discussed in the next section.

288 For tissue stiffness parameters, although reliability was not satisfactory for all three parameters: skin, hypodermis, and
289 muscle; the 95% CI level of agreement with the mean of the inter-image analysis of ± 0.33 m/s; ± 0.29 m/s; ± 0.25 m/s
290 respectively, was minimal. In fact, previous studies investigating changes of shear wave velocity values in specific
291 circumstances or disease showed: with prolonged loading in elderly, shear wave velocity of superficial region (mainly
292 skin + hypodermis) over IT varied from 2.5 m/s to 3.3 m/s [31]; contracture strips of the gluteal muscle showed a shear
293 wave velocity of 7.23 m/s vs 1.84 m/s for a healthy muscle at the same position[47]. Because the aim of this evaluation
294 is to point out subjects who significantly diverge from normal values, the SWE values for the three regions remain
295 interesting to report. Nevertheless, interpretation should be taken with caution and further investigations are needed to
296 increase reliability. Possible solutions might include operator's training, and taking SWE videos in the transverse and
297 vertical directions, especially for muscle stiffness, since the properties parallel to the fibers are quite different from
298 loading perpendicular to the fibers [48].

299

300 **2. Young adults vs healthy elderly**

301 The following discussion will highlight observations noted when comparing parameters of the young adults group and
302 the healthy older people for the acquisitions conducted only by the physician. The interpretations cannot be generalized
303 since reliability of measurements was not satisfactory.

304 For bone parameters, aging is associated with structural, geometric and bone volumetric density changes [49]. It is
305 unclear how that might affect the external shape of the MSC; the similar median values in the boxplot, and the absence
306 of statistical significance of differences between the means for the three parameters might suggest that there are no
307 US changes observable. Therefore, the estimation of these parameters aims to evaluate the impact of bone geometry
308 on tissue deformation independently from age difference.

309 For the tissue morphology parameters, the median values for both ST and HT were lower for the older group, but no
310 statistical difference was noted between means. In fact, studies have shown that thinning of the skin, associated with
311 age, is observed in subjects with more than 70 years [50] while our older age group had a mean age of 65 ± 2.4 yrs.
312 Nevertheless, the mean ST of the young adults group 3.61 ± 0.55 mm was close to values previously reported for the

313 skin over the sacrum like, for example, Yalcin et al [51] found a mean of 3.2 ± 0.5 mm. Also studies comparing tissue
314 thickness differences between SCI patients without vs with history of PU showed total thickness average of 15.3 mm
315 vs 9.5 mm over the apex of IT [25]. Thus, the difference is quantifiable, but the challenge remains to determine a risk
316 threshold value at high-risk patients. On the other hand, an observation, not reported in the literature to our knowledge,
317 was noted for the hypodermis thickness distribution over the sacrum. One subject (fig.2b) clearly showed thinning of
318 HT from the lateral to medial spine. Possible causes might be a spinal deformation causing a shift in the hypodermis
319 layer while the skin, loosely bonded to subjacent organs, can slide over and maintain the same thickness [39]. This
320 highlights the importance of measuring the HT directly over the tip of the MSC instead of the thickest region as
321 mentioned in our protocol. In fact, HT is considered as an important parameter affecting internal soft tissue response
322 to load [23] and thus, PU risk.

323 For the tissue stiffness parameters, median shear wave velocity for skin, hypodermis, and muscle was lower for the
324 elderly group. Only for the muscle the difference showed statistical significance ($p=0.001$). In fact, physiologic aging
325 is associated with a loss of muscle mass starting at the age of 30 [10]. This might be caused by the infiltration of fat
326 tissue and connective tissue into skeletal muscle [52]. Previous studies suggest that this is associated with an increase
327 in muscle stiffness [53] and, with continuous compression, a further increase in muscle stiffness leading to injury [54].
328 While our results seem contradictory, since we noted a decrease in shear wave velocity between the young and the
329 elderly group, the signal was collected closer to the proximal attachment of the gluteus maximus (lateral to the sacro-
330 coccygeal region) rather than the muscle belly. Moreover, most studies, evaluating tissue stiffness and PU, focused on
331 the variation of stiffness with loading [31], [54], [55]. The complexity and duration of the exam, especially for high-
332 risk subjects, makes it impossible to evaluate a large number in a loading position. That is why we proposed in our
333 study to evaluate tissue characteristics in an off-loading position and determine normal ranges within homogenous
334 groups. While studies suggest that aging is associated with a decline in skin stiffness [9], [56] making it more
335 susceptible to PU, there is no specific threshold value proposed for increased risk. On the other hand, sustained
336 pressure application was associated with an increase in tissue stiffness [31], [57], [58]. The two subjects presenting
337 maximum and minimum skin/hypodermis baseline shear wave velocity in the elderly group (fig2.a; fig2.b) were
338 overweight ($BMI > 25$ kg/m²). It is known that BMI values have an impact on the biomechanical behavior of tissues
339 [59], [60], further investigations are needed to evaluate changes in tissue elasticity associated with BMI changes. Also
340 the mean values of sSWE and hSWE over the sacrum of the elderly group (2.22 ± 0.55 m/s and 1.98 ± 0.33 m/s

341 respectively) are close to values reported in the literature (2.5 m/s and 1.8 m/s respectively) for a similar sample of
342 nine healthy volunteers with a mean age of 70.1 ± 4.8 years [31].

343

344 **3. Limits and perspectives**

345 The lack of reliability of measures is the main limit of our study. This is mainly related to: difficulty in repeating
346 acquisitions on the same anatomic level, definition of parameters, lack of signal stability, and ultrasound expertise.

347 Also, the patient's prone position might be problematic for higher risk subjects. The sample size and the number of
348 operators is also a limitation of this study. However, the protocol we developed is clinically feasible and can be easily
349 proposed to evaluate patients at bedside. The relatively easy palpation of the anatomic landmark (PSIS) allows the
350 exam to be conducted by any physician or nurse. The perspectives include a review of the protocol to increase
351 reliability and an evaluation of higher risk elderly in nursing homes. Also, this protocol can quantify all layers'
352 characteristics including bone, muscle, hypodermis, and skin using only US and SWE. This might serve in - patient
353 specific - finite element modeling since quantifying tissue strain and stress distribution over a bony prominence is
354 essential in determining an injury threshold [23], [55], [61].

355

356 **Conclusion**

357 In this study, we developed a protocol using US and SWE to assess bone and tissue characteristics over the sacrum in
358 the context of PU prevention in elderly. It is the first protocol that combines assessment of all layers over bony
359 prominences using only one imaging technique.

360 The protocol's reliability was evaluated on a sample of young adults and then tested on a group of healthy older
361 subjects. We provided a thorough description of anatomic landmarks on palpation and US visualization to ensure
362 reproducibility and real clinical application. However, reliability was not satisfactory and further improvements of the
363 protocol are needed. The results comparing the young to healthy older age group suggested that changes related only
364 to age might affect tissue thickness and elasticity more than bone morphology, but this cannot be generalized or
365 quantified before increasing reliability and sample size. On the other hand, an observation in one of the subjects of the
366 elderly group was not found in the literature: a heterogeneous distribution of the hypodermis thickness over the

367 sacrum. In order to evaluate the use of this tool for PU risk assessment, it is essential to test it on a high-risk sample
368 like elderly in nursing homes or long hospital stay.

369 Finally, our recommendations for the scientific community - when using US and SWE – are:

- 370 - anatomic palpation and US recognition using the curvilinear probe.
- 371 - report exact anatomic region and provide proof on the US image.
- 372 - when measuring thickness and SWE ensure that acquisition is taken pressure free directly over the bone
373 prominence and not in the surrounding region.
- 374 - results cannot be generalized before testing for reliability.

375

376 **Acknowledgement**

377 This project has received funding from the European Union’s Horizon 2020 research and innovation program under
378 the Marie Skłodowska-Curie grant agreement No. 811965.

379

380 **Conflict of interest**

381 None

382

383 **APPENDIX 1**

384 **Ultrasound and SWE protocol**

385 *Position and anatomic landmarks*

386 The volunteer is asked to lie down in the prone position with a cushion under the pubis to reduce lumbar lordosis. The
387 examiner inspects the skin to identify any redness/swelling over the sacral region. Then, he palpates the posterior
388 superior iliac spine (PSIS) and recognizes the continuation of intergluteal cleft representing the midline of the spine.

389

390

391

392 *Curvilinear probe*

393 The curvilinear probe allows a large field of view and better visualization of deep layers. After applying gel on the
394 skin or the probe, the examiner scans the sacral region between the two PSIS in B-mode transverse view. The MSC
395 appears as a reverse V-shaped hyperechoic contour (fig.1a). Sliding the probe lateral to the midline allows the
396 recognition of the round shaped PSIS (fig.1a). An image is captured showing the MSC and PSIS. The region is marked
397 over the skin with a marker or medical tape.

398 NB: if PSIS is not visible on US the use of sagittal view of the sacrum allows to recognize the anatomic site of the
399 MSC. The examiner can align the site in the middle of the US image and then rotate the probe 90 degrees to return to
400 transverse view.

401 *Linear probe*

402 The linear probe is used to assess the superficial layers over the MSC. A thick layer of gel is applied directly on the
403 midline of the marked level. The probe is then applied in the transverse B-mode view with minimum pressure.
404 Artefacts from air bubbles appear as a linear hypoechoic signal perpendicular to skin layers. The examiner eliminates
405 air bubbles using the probe or by adding and spreading the gel again. An image is captured showing the skin and
406 adipose tissue, and the thick layer of gel over the skin (fig.1b).

407 The linear probe is also used in SWE mode at the same level with a thick gel layer and minimum pressure. The region
408 of interest (ROI) covering the skin and adipose tissue is chosen, and the examiner waits for a homogeneous signal on
409 the screen, increasing/decreasing elasticity range matching tissue stiffness. One measurement is three videos in SWE
410 of 10 seconds each (or more if signal fluctuates). The last acquisition in SWE mode, for the gluteus maximus muscle,
411 is taken lateral to the sacro-coccygeal region using the same procedure. The anatomic landmark is the sacral horns
412 and sacro-coccygeal ligament described as the “frog sign”. The muscle fibers are described as horizontal echoic lines
413 under the skin and hypodermis (fig1.c).

414

415

416

417

418 References

- 419 [1] NPIAP/EPUAP/PPPIA, *Prevention and Treatment of Pressure Ulcers/Injuries: Clinical practice Guideline. The*
420 *International Guideline.*, Emily Haesler. Australia, 2019.
- 421 [2] Z. Moore and S. Cowman, "Pressure ulcer prevalence and prevention practices in care of the older person in the Republic
422 of Ireland," *Journal of Clinical Nursing*, vol. 21, no. 3–4, pp. 362–371, 2012, doi: [https://doi.org/10.1111/j.1365-](https://doi.org/10.1111/j.1365-2702.2011.03749.x)
423 [2702.2011.03749.x](https://doi.org/10.1111/j.1365-2702.2011.03749.x).
- 424 [3] T. E. Børsting, C. R. Tvedt, I. J. Skogestad, T. I. Granheim, C. L. Gay, and A. Lerdal, "Prevalence of pressure ulcer and
425 associated risk factors in middle- and older-aged medical inpatients in Norway," *Journal of Clinical Nursing*, vol. 27, no.
426 3–4, pp. e535–e543, Feb. 2018, doi: [10.1111/jocn.14088](https://doi.org/10.1111/jocn.14088).
- 427 [4] K. Agrawal and N. Chauhan, "Pressure ulcers: Back to the basics," *Indian J Plast Surg*, vol. 45, no. 2, pp. 244–254, 2012,
428 doi: [10.4103/0970-0358.101287](https://doi.org/10.4103/0970-0358.101287).
- 429 [5] R. M. Allman, P. S. Goode, N. Burst, A. A. Bartolucci, and D. R. Thomas, "Pressure ulcers, hospital complications, and
430 disease severity: impact on hospital costs and length of stay," *Adv Wound Care*, vol. 12, no. 1, pp. 22–30, Feb. 1999.
- 431 [6] M. Situm, M. Kolić, and S. Spoljar, "[QUALITY OF LIFE AND PSYCHOLOGICAL ASPECTS IN PATIENTS WITH
432 CHRONIC LEG ULCER]," *Acta Med Croatica*, vol. 70, no. 1, pp. 61–63, Mar. 2016.
- 433 [7] Z. E. Moore and D. Patton, "Risk assessment tools for the prevention of pressure ulcers," *Cochrane Database Syst Rev*,
434 vol. 2019, no. 1, Jan. 2019, doi: [10.1002/14651858.CD006471.pub4](https://doi.org/10.1002/14651858.CD006471.pub4).
- 435 [8] K. Balzer, C. Pohl, T. Dassen, and R. Halfens, "The Norton, Waterlow, Braden, and Care Dependency Scales: comparing
436 their validity when identifying patients' pressure sore risk," *J Wound Ostomy Continence Nurs*, vol. 34, no. 4, pp. 389–
437 398, Aug. 2007, doi: [10.1097/01.WON.0000281655.78696.00](https://doi.org/10.1097/01.WON.0000281655.78696.00).
- 438 [9] G. R. Boss and J. E. Seegmiller, "Age-Related Physiological Changes and Their Clinical Significance," *West J Med*, vol.
439 135, no. 6, pp. 434–440, Dec. 1981.
- 440 [10] C. A. Harms, D. Cooper, and H. Tanaka, "Exercise physiology of normal development, sex differences, and aging,"
441 *Compr Physiol*, vol. 1, no. 4, pp. 1649–1678, Oct. 2011, doi: [10.1002/cphy.c100065](https://doi.org/10.1002/cphy.c100065).
- 442 [11] A. L. Oliveira, Z. Moore, T. O Connor, and D. Patton, "Accuracy of ultrasound, thermography and subepidermal moisture
443 in predicting pressure ulcers: a systematic review," *J Wound Care*, vol. 26, no. 5, pp. 199–215, May 2017, doi:
444 [10.12968/jowc.2017.26.5.199](https://doi.org/10.12968/jowc.2017.26.5.199).
- 445 [12] S. Grubbs *et al.*, "The Effect of High Frequency Ultrasound on the Prevention of Pressure Ulcers in Long-term Care
446 Patients," *The Internet Journal of Academic Physician Assistants*, vol. 7, no. 1, Dec. 2008, Accessed: Jul. 14, 2021.
447 [Online]. Available: <https://ispub.com/IJAPA/7/1/11804>
- 448 [13] K. N. Scafide, M. C. Narayan, and L. Arundel, "Bedside Technologies to Enhance the Early Detection of Pressure
449 Injuries: A Systematic Review," *Journal of Wound Ostomy & Continence Nursing*, vol. 47, no. 2, pp. 128–136, Apr. 2020,
450 doi: [10.1097/WON.0000000000000626](https://doi.org/10.1097/WON.0000000000000626).
- 451 [14] C. w. j. Oomens, M. Broek, B. Hemmes, and D. l. Bader, "How does lateral tilting affect the internal strains in the sacral
452 region of bed ridden patients? — A contribution to pressure ulcer prevention," *Clinical Biomechanics*, vol. 35, pp. 7–13,
453 Jun. 2016, doi: [10.1016/j.clinbiomech.2016.03.009](https://doi.org/10.1016/j.clinbiomech.2016.03.009).
- 454 [15] A. Levy, K. Kopplin, and A. Gefen, "An air-cell-based cushion for pressure ulcer protection remarkably reduces tissue
455 stresses in the seated buttocks with respect to foams: Finite element studies," *Journal of Tissue Viability*, vol. 23, no. 1, pp.
456 13–23, Feb. 2014, doi: [10.1016/j.jtv.2013.12.005](https://doi.org/10.1016/j.jtv.2013.12.005).

- 457 [16] R. M. A. Al-Dirini, M. P. Reed, J. Hu, and D. Thewlis, "Development and Validation of a High Anatomical Fidelity FE
458 Model for the Buttock and Thigh of a Seated Individual," *Ann Biomed Eng*, vol. 44, no. 9, pp. 2805–2816, Sep. 2016, doi:
459 10.1007/s10439-016-1560-3.
- 460 [17] V. Luboz, M. Petrizelli, M. Bucki, B. Diot, N. Vuillerme, and Y. Payan, "Biomechanical modeling to prevent ischial
461 pressure ulcers," *J Biomech*, vol. 47, no. 10, pp. 2231–2236, Jul. 2014, doi: 10.1016/j.jbiomech.2014.05.004.
- 462 [18] E. Linder-Ganz, N. Shabshin, Y. Itzchak, and A. Gefen, "Assessment of mechanical conditions in sub-dermal tissues
463 during sitting: A combined experimental-MRI and finite element approach," *Journal of Biomechanics*, vol. 40, no. 7, pp.
464 1443–1454, Jan. 2007, doi: 10.1016/j.jbiomech.2006.06.020.
- 465 [19] J. S. Akins *et al.*, "Feasibility of freehand ultrasound to measure anatomical features associated with deep tissue injury
466 risk," *Med Eng Phys*, vol. 38, no. 9, pp. 839–844, Sep. 2016, doi: 10.1016/j.medengphy.2016.04.026.
- 467 [20] J. M. Swaine *et al.*, "Adaptation of a MR imaging protocol into a real-time clinical biometric ultrasound protocol for
468 persons with spinal cord injury at risk for deep tissue injury: A reliability study," *Journal of Tissue Viability*, vol. 27, no.
469 1, pp. 32–41, Feb. 2018, doi: 10.1016/j.jtv.2017.07.004.
- 470 [21] A. Macron, H. Pillet, J. Doridam, A. Verney, and P.-Y. Rohan, "Development and evaluation of a new methodology for
471 the fast generation of patient-specific Finite Element models of the buttock for sitting-acquired deep tissue injury
472 prevention," *Journal of Biomechanics*, vol. 79, pp. 173–180, Oct. 2018, doi: 10.1016/j.jbiomech.2018.08.001.
- 473 [22] J. Doridam, A. Macron, C. Vergari, A. Verney, P.-Y. Rohan, and H. Pillet, "Feasibility of sub-dermal soft tissue
474 deformation assessment using B-mode ultrasound for pressure ulcer prevention," *J Tissue Viability*, vol. 27, no. 4, pp.
475 238–243, Nov. 2018, doi: 10.1016/j.jtv.2018.08.002.
- 476 [23] A. Macron *et al.*, "Is a simplified Finite Element model of the gluteus region able to capture the mechanical response of
477 the internal soft tissues under compression?," *Clinical Biomechanics*, vol. 71, pp. 92–100, Jan. 2020, doi:
478 10.1016/j.clinbiomech.2019.10.005.
- 479 [24] S. Gabison, K. Hayes, K. E. Campbell, J. M. Swaine, and B. C. Craven, "Ultrasound imaging of tissue overlying the
480 ischial tuberosity: Does patient position matter?," *Journal of Tissue Viability*, vol. 28, no. 4, pp. 179–185, Nov. 2019, doi:
481 10.1016/j.jtv.2019.07.001.
- 482 [25] S. E. Sonenblum, D. Seol, S. H. Sprigle, and J. M. Cathcart, "Seated buttocks anatomy and its impact on biomechanical
483 risk," *Journal of Tissue Viability*, Jan. 2020, doi: 10.1016/j.jtv.2020.01.004.
- 484 [26] Ł. Paluch, E. Nawrocka-Laskus, J. Wiczorek, B. Mruk, M. Frel, and J. Walecki, "Use of Ultrasound Elastography in the
485 Assessment of the Musculoskeletal System," *Pol J Radiol*, vol. 81, pp. 240–246, May 2016, doi: 10.12659/PJR.896099.
- 486 [27] J. Bercoff, M. Tanter, and M. Fink, "Supersonic shear imaging: a new technique for soft tissue elasticity mapping," *IEEE*
487 *Transactions on Ultrasonics, Ferroelectrics, and Frequency Control*, vol. 51, no. 4, pp. 396–409, Apr. 2004, doi:
488 10.1109/TUFFC.2004.1295425.
- 489 [28] J.-F. Deprez, E. Brusseau, J. Fromageau, G. Cloutier, and O. Basset, "On the potential of ultrasound elastography for
490 pressure ulcer early detection," *Medical Physics*, vol. 38, no. 4, pp. 1943–1950, 2011, doi: 10.1118/1.3560421.
- 491 [29] G. Dubois *et al.*, "Reliable protocol for shear wave elastography of lower limb muscles at rest and during passive
492 stretching," *Ultrasound Med Biol*, vol. 41, no. 9, pp. 2284–2291, Sep. 2015, doi: 10.1016/j.ultrasmedbio.2015.04.020.
- 493 [30] R. M. S. Sigrist, J. Liau, A. E. Kaffas, M. C. Chammas, and J. K. Willmann, "Ultrasound Elastography: Review of
494 Techniques and Clinical Applications," *Theranostics*, vol. 7, no. 5, pp. 1303–1329, 2017, doi: 10.7150/thno.18650.
- 495 [31] G. Schäfer, G. Dobos, L. Lünemann, U. Blume-Peytavi, T. Fischer, and J. Kottner, "Using ultrasound elastography to
496 monitor human soft tissue behaviour during prolonged loading: A clinical explorative study," *Journal of Tissue Viability*,
497 vol. 24, no. 4, pp. 165–172, Nov. 2015, doi: 10.1016/j.jtv.2015.06.001.

- 498 [32] R. Mansur, L. Peko, N. Shabshin, L. Cherbinski, Z. Neeman, and A. Gefen, "Ultrasound elastography reveals the relation
499 between body posture and soft-tissue stiffness which is relevant to the etiology of sitting-acquired pressure ulcers,"
500 *Physiol. Meas.*, vol. 41, no. 12, p. 124002, Jan. 2021, doi: 10.1088/1361-6579/abc66d.
- 501 [33] C. Vergari *et al.*, "Intervertebral disc characterization by shear wave elastography: An in vitro preliminary study," *Proc*
502 *Inst Mech Eng H*, vol. 228, no. 6, pp. 607–615, Jun. 2014, doi: 10.1177/0954411914540279.
- 503 [34] K. McGraw and S. P. Wong, "Forming Inferences About Some Intraclass Correlation Coefficients," *Psychological*
504 *Methods*, vol. 1, pp. 30–46, Mar. 1996, doi: 10.1037/1082-989X.1.1.30.
- 505 [35] M. A. Bujang, "A simplified guide to determination of sample size requirements for estimating the value of intraclass
506 correlation coefficient: A review," *Archives of Orofacial Sciences*, vol. 12, pp. 1–11, Jun. 2017.
- 507 [36] J. J. Hebert, S. L. Koppenhaver, E. C. Parent, and J. M. Fritz, "A systematic review of the reliability of rehabilitative
508 ultrasound imaging for the quantitative assessment of the abdominal and lumbar trunk muscles," *Spine (Phila Pa 1976)*,
509 vol. 34, no. 23, pp. E848–856, Nov. 2009, doi: 10.1097/BRS.0b013e3181ae625c.
- 510 [37] T. K. Koo and M. Y. Li, "A Guideline of Selecting and Reporting Intraclass Correlation Coefficients for Reliability
511 Research," *J Chiropr Med*, vol. 15, no. 2, pp. 155–163, Jun. 2016, doi: 10.1016/j.jcm.2016.02.012.
- 512 [38] M. Jones, A. Dobson, and S. O'Brian, "A graphical method for assessing agreement with the mean between multiple
513 observers using continuous measures," *International Journal of Epidemiology*, vol. 40, no. 5, pp. 1308–1313, Oct. 2011,
514 doi: 10.1093/ije/dyr109.
- 515 [39] "Skin. Mescher A.L.(Ed.)," in *Junqueira's Basic Histology Text and Atlas, 16e*, Book, Section vols., New York, NY:
516 McGraw Hill, 2021. Accessed: May 17, 2021. [Online]. Available:
517 accessmedicine.mhmedical.com/content.aspx?aid=1180414032
- 518 [40] J. S. Cheng and J. K. Song, "Anatomy of the sacrum," *Neurosurgical Focus*, vol. 15, no. 2, pp. 1–4, Aug. 2003, doi:
519 10.3171/foc.2003.15.2.3.
- 520 [41] M.-P. Baron-Sarrabère, A. Micheau, and C. Cyteval, "Sacrum, coccyx, articulations sacro-iliaques : technique
521 radiologique et aspects normaux," [//www.em-premium.com/data/traites/rx/30-60680/](http://www.em-premium.com/data/traites/rx/30-60680/), Sep. 2016, Accessed: Dec. 27,
522 2021. [Online]. Available: <https://ezproxy.usj.edu.lb:2170/article/1083162>
- 523 [42] M. Serafin-Król and A. Maliborski, "Diagnostic errors in musculoskeletal ultrasound imaging and how to avoid them," *J*
524 *Ultrasound*, vol. 17, no. 70, pp. 188–196, Sep. 2017, doi: 10.15557/JoU.2017.0028.
- 525 [43] A. Gefen, "Risk factors for a pressure-related deep tissue injury: a theoretical model," *Med Bio Eng Comput*, vol. 45, no.
526 6, pp. 563–573, Jun. 2007, doi: 10.1007/s11517-007-0187-9.
- 527 [44] R. S. Candadai and N. P. Reddy, "Stress distribution in a physical buttock model: Effect of simulated bone geometry,"
528 *Journal of Biomechanics*, vol. 25, no. 12, pp. 1403–1411, Dec. 1992, doi: 10.1016/0021-9290(92)90054-5.
- 529 [45] M. A. Gibney, C. H. Arce, K. J. Byron, and L. J. Hirsch, "Skin and subcutaneous adipose layer thickness in adults with
530 diabetes at sites used for insulin injections: implications for needle length recommendations," *Current Medical Research*
531 *and Opinion*, vol. 26, no. 6, pp. 1519–1530, Jun. 2010, doi: 10.1185/03007995.2010.481203.
- 532 [46] J. J. Lee *et al.*, "Fat Thickness as a Risk Factor for Infection in Lumbar Spine Surgery," *Orthopedics*, vol. 39, no. 6, pp.
533 e1124–e1128, Nov. 2016, doi: 10.3928/01477447-20160819-05.
- 534 [47] R. Guo, X. Xiang, and L. Qiu, "Shear-wave elastography assessment of gluteal muscle contracture," *Medicine*
535 *(Baltimore)*, vol. 97, no. 44, Nov. 2018, doi: 10.1097/MD.0000000000013071.
- 536 [48] P. Escobar, S. Wittles, S. Asfour, and L. Latta, "Mechanical Characteristics of Muscle, Skin and Fat - Elastic Moduli for
537 Finite Element Modeling of Limbs," p. 4.

- 538 [49] B. L. Riggs *et al.*, “Population-Based Study of Age and Sex Differences in Bone Volumetric Density, Size, Geometry, and
539 Structure at Different Skeletal Sites,” *Journal of Bone and Mineral Research*, vol. 19, no. 12, pp. 1945–1954, Dec. 2004,
540 doi: 10.1359/jbmr.040916.
- 541 [50] C. Lasagni and S. Seidenari, “Echographic assessment of age-dependent variations of skin thickness,” *Skin Research and*
542 *Technology*, vol. 1, no. 2, pp. 81–85, 1995, doi: 10.1111/j.1600-0846.1995.tb00022.x.
- 543 [51] E. Yalcin, M. Akyuz, B. Onder, H. Unalan, and I. Degirmenci, “Skin thickness on bony prominences measured by
544 ultrasonography in patients with spinal cord injury,” *J Spinal Cord Med*, vol. 36, no. 3, pp. 225–230, May 2013, doi:
545 10.1179/2045772312Y.0000000088.
- 546 [52] R. McCormick and A. Vasilaki, “Age-related changes in skeletal muscle: changes to life-style as a therapy,”
547 *Biogerontology*, vol. 19, no. 6, pp. 519–536, 2018, doi: 10.1007/s10522-018-9775-3.
- 548 [53] H. Rahemi, N. Nigam, and J. M. Wakeling, “The effect of intramuscular fat on skeletal muscle mechanics: implications
549 for the elderly and obese,” *J R Soc Interface*, vol. 12, no. 109, p. 20150365, Aug. 2015, doi: 10.1098/rsif.2015.0365.
- 550 [54] A. Gefen, N. Gefen, E. Linder-Ganz, and S. S. Margulies, “In Vivo Muscle Stiffening Under Bone Compression Promotes
551 Deep Pressure Sores,” *Journal of Biomechanical Engineering*, vol. 127, no. 3, pp. 512–524, Jan. 2005, doi:
552 10.1115/1.1894386.
- 553 [55] E. Linder-Ganz, N. Shabshin, Y. Itzchak, Z. Yizhar, I. Siev-Ner, and A. Gefen, “Strains and stresses in sub-dermal tissues
554 of the buttocks are greater in paraplegics than in healthy during sitting,” *Journal of Biomechanics*, vol. 41, no. 3, pp. 567–
555 580, 2008, doi: 10.1016/j.jbiomech.2007.10.011.
- 556 [56] S. Luebberding, N. Krueger, and M. Kerscher, “Mechanical properties of human skin in vivo: a comparative evaluation in
557 300 men and women,” *Skin Research and Technology*, vol. 20, no. 2, pp. 127–135, May 2014, doi: 10.1111/srt.12094.
- 558 [57] A. Gefen, “The biomechanics of sitting-acquired pressure ulcers in patients with spinal cord injury or lesions,”
559 *International Wound Journal*, vol. 4, no. 3, pp. 222–231, 2007, doi: 10.1111/j.1742-481X.2007.00330.x.
- 560 [58] N. Shoham and A. Gefen, “Deformations, mechanical strains and stresses across the different hierarchical scales in
561 weight-bearing soft tissues,” *Journal of Tissue Viability*, vol. 21, no. 2, pp. 39–46, May 2012, doi:
562 10.1016/j.jtv.2012.03.001.
- 563 [59] R. Sopher, J. Nixon, C. Gorecki, and A. Gefen, “Exposure to internal muscle tissue loads under the ischial tuberosities
564 during sitting is elevated at abnormally high or low body mass indices,” *Journal of Biomechanics*, vol. 43, no. 2, pp. 280–
565 286, Jan. 2010, doi: 10.1016/j.jbiomech.2009.08.021.
- 566 [60] J. J. Elsner and A. Gefen, “Is obesity a risk factor for deep tissue injury in patients with spinal cord injury?,” *Journal of*
567 *Biomechanics*, vol. 41, no. 16, pp. 3322–3331, Dec. 2008, doi: 10.1016/j.jbiomech.2008.09.036.
- 568 [61] S. Loerakker *et al.*, “The effects of deformation, ischemia, and reperfusion on the development of muscle damage during
569 prolonged loading,” *Journal of Applied Physiology*, vol. 111, no. 4, pp. 1168–1177, Jul. 2011, doi:
570 10.1152/jappphysiol.00389.2011.

571

572

573

574

575

576

577

List of figures

| | |
|----------|--|
| Figure 1 | US acquisition protocol of the sacral region in the transverse view. In B-mode: the medial sacral crest (arrow) at the level of the PSIS (black triangle) (a), skin (arrow) and adipose tissue (white triangle) over MSC (b); in SWE mode: the skin and adipose tissue (c), gluteus maximus muscle (star) (d). |
| Figure 2 | Agreement plots with the mean of measurements for the intra-image and inter-image analyses for the 8 parameters. |
| Figure 3 | Observations in the older group: lowest and highest skin/hypodermis SWE signal (a,b respectively), hypodermis heterogeneous thickness distribution over the MSC (double arrow) (c). |

578

579

List of tables

| | |
|---------|--|
| Table 1 | Description of parameter measurement post acquisition using a customized MATLAB algorithm |
| Table 2 | Reliability assessment results with Intraclass correlation coefficient ICC for both intra-image and inter-image analysis for both operators: 1 the physician and 2 the engineer. |
| Table 3 | Mean of each parameter for the young adults group and healthy elderly, normality using Shapiro-wilk test and comparison using Student's t-test |

580